Antiprotons from spallations of cosmic rays on interstellar matter

F. Donato[1]

Laboratoire de Physique Théorique LAPTH, *Annecy–le–Vieux, 74941, France*

donato@lapp.in2p3.fr

D. Maurin and P. Salati[2]

Laboratoire de Physique Théorique LAPTH, *Annecy–le–Vieux, 74941, France*
Université de Savoie, Chambéry, 73011, France

maurin@lapp.in2p3.fr, salati@lapp.in2p3.fr

A. Barrau and G. Boudoul

Institut des Sciences Nucléaires ISN, *Grenoble, 38026, France*
Université Joseph Fourier, St Martin d'Hères, 38400, France

barrau@isn.in2p3.fr, boudoul@isn.in2p3.fr

and

R. Taillet

Laboratoire de Physique Théorique LAPTH, *Annecy–le–Vieux, 74941, France*
Université de Savoie, Chambéry, 73011, France.

taillet@lapp.in2p3.fr

ABSTRACT

Cosmic ray antiprotons provide an important probe for the study of the galactic Dark Matter, as they could be produced by neutralino annihilations, primordial black holes evaporations or other exotic sources. On the other hand, antiprotons are anyway produced by standard nuclear reactions of cosmic ray nuclei on interstellar matter (*spallations*), that are known to occur in the Galaxy. This process is responsible for a background flux that must be carefully determined to estimate the detectability of an hypothetical exotic signal.

[1] INFN post–doctoral Fellow

In this paper we provide a new evaluation of the interstellar cosmic antiproton flux that is fully consistent with cosmic ray nuclei in the framework of a two-zone diffusion model. We also study and conservatively quantify all possible sources of uncertainty that may affect that antiproton flux. In particular, the primary cosmic rays are by now so well measured that the corresponding error is removed. Uncertainties related to propagation are shown to range between 10% and 25%, depending on which part of the spectrum is considered.

1. Introduction

The study of the cosmic ray antiproton spectrum has been a great challenge since the first measurements made at the end of the seventies. Actually, the first experiments provided data which, in the low energy tail, showed some excess when compared to the current model predictions. This discrepancy stimulated a great interest into alternative explanations, viz the possible existence of primary antiproton sources. Such an interest did not fade even when further experimental data seemed to agree with theoretical predictions in standard leaky box models (see for example Stephens & Golden 1988 and references therein).

Various primary antiproton sources have been proposed (Silk & Srednicki 1984; Stecker, Rudaz, & Walsh 1985; Ellis et al. 1988; Starkman & Vachaspati 1996; Mitsui, Maki, & Orito 1996). The case of supersymmetric sources – relic neutralinos in the galactic halo – has received a particular attention and constraints on SUSY parameters have been investigated by comparing experimental data to theoretical predictions (Bottino et al. 1995; Chardonnet et al. 1996; Bottino et al. 1998; Bergström, Edsjö, & Ullio 1999). However, an important problem with this comparison is that an accurate estimation of the background secondary antiproton flux produced by spallations is mandatory.

In this paper, we focus on this secondary antiproton flux, which we will call "background" antiproton flux, having in mind the possibility of using it to determine whether one of the primary components ("signal") discussed above could be seen against it or not (P. Salati & al, in preparation; A. Barrau & al, in preparation). Such hypothetical signals will not be further discussed in this paper. We believe that now is a good time for a detailed evaluation of the background flux, since the next measurements of $\bar{p}$ spectra should be very accurate at low energy ($\sim$ 100 MeV $-$ 10 GeV) especially in the forthcoming ten years (AMS, BESS, PAMELA, ...). On the theoretical side, progress has already been made in many directions. Here are some milestones on the way: (i) the inelastic non-annihilating cross-section for $\bar{p}$ (Tan & Ng 1982, 1983), giving rise to the so–called tertiary contribution, has been taken into account (ii) the $p + He_{\rm ISM} \rightarrow \bar{p}$ contribution has been considered by

means of a simple geometric approach (Gaisser & Schaefer 1992), (iii) reacceleration has been considered (Simon & Heinbach 1996), (iv) propagation has been modeled in a more realistic two–zone diffusion model (Halm, Jansen, & de Niem 1993; Chardonnet et al. 1996), (v) the $(p, He) + (H, He)_{\rm ISM}$ reactions have been re-estimated in a more sophisticated nuclear Monte Carlo (Simon, Molnar, & Roesler 1998), (vi) the great variety of cosmic rays has been treated in a more coherent way (Moskalenko, Strong & Reimer 1998). As far as we know, all these ingredients have only been considered simultaneously in Moskalenko et al. 1998 (see also Moskalenko et al. 2001).

We propose to go beyond this type of study and to use the results of our systematic analysis of nuclei (Maurin et al. 2001, referred hereafter as Paper I) to ascertain the theoretical uncertainties on the interstellar secondary antiproton energy spectrum. This goal has never been achieved before, even in Moskalenko et al. 1998, 2001. The paper is organized as follows. Separate sections are devoted to all the ingredients entering the calculation of the $\bar{p}$ background: measured H and He flux, secondary production, tertiary contribution and propagation. Whithin each section, we first discuss the model used and the associated parameters; then we estimate the uncertainty they induce in the $\bar{p}$ background. An important aspect is worth a warning at this point. As will be discussed in section 6, the effect of solar modulation may be decoupled from the problem of interstellar propagation and this problem will not be addressed here. When a modulated flux is needed, we will use a simple force-field approximation modulation scheme, as in most cosmic antiprotons studies. Would a more careful treatment of solar modulation be needed (see for example Bieber et al. 1999), an interstellar flux can easily be obtained by demodulation (the force-field approximation modulation scheme is reversible). This interstellar flux could then be used as an input for any other preferred treatment of solar modulation.

To sum up, we used results from a systematic nuclei cosmic ray analysis to consistently derive an antiproton secondary flux in the framework of diffusion models. As an important consequence we could study and quantify most of the uncertainties: in the propagation, in the nuclear physics and in the primary cosmic ray. We feel that our results will be valuable not only for speculations on primary contributions to that flux but also for the experimental groups which are going to perform very accurate antiproton measurements in the near future.

2. Proton and Helium primary spectra

The secondary antiprotons are yielded by the spallation of cosmic ray nuclei over the interstellar medium (see Appendix A for the formulæ). The most abundant species in cosmic rays are protons and helium, and the contribution of heavier nuclei to the antiproton pro-

duction is negligible. Until recently, their spectra were known with a modest accuracy and the data from different experiments were often incompatible at high energy. This induced an uncertainty of some tens of percents in the predicted antiproton spectrum. Recent measurements made by the balloon–borne spectrometer BESS (Sanuki et al. 2000) and by the AMS detector during the space shuttle flight (Alcaraz et al. 2000a, 2000b, 2000c) dramatically reduced the uncertainties both on proton and helium spectra. We fitted the high energy (T $>$ 20 GeV/n) part of these measured spectra with the power law:

$$\Phi(\mathrm{T}) = \mathrm{N}\,(\mathrm{T}/\ \mathrm{GeV/n})^{-\gamma}\ \ , \tag{1}$$

where the kinetic energy per nucleon T is given in units of GeV/n and the normalization factor N in units of $\mathrm{m^{-2}\ s^{-1}\ sr^{-1}\ (GeV/n)^{-1}}$. This provides a good description down to the threshold energy for the antiproton production.

We fitted the BESS and AMS data both separately and combined, obtaining very similar results. This is obvious since the data from the two experiments are now totally compatible, as can be seen in Fig. 1. The upper curve presents our fit on the combined proton data. The best fit corresponds to $N = 13249\ \mathrm{m^{-2}\ s^{-1}\ sr^{-1}\ (GeV/n)^{-1}}$ and $\gamma = 2.72$. We do not plot the spectra obtained from the best fits on the single BESS and AMS data because of their complete overlap with the plotted curve. We did the same for helium (lower curve) and the corresponding numbers are $N = 721\ \mathrm{m^{-2}\ s^{-1}\ sr^{-1}\ (GeV/n)^{-1}}$ and $\gamma = 2.74$. The 1–σ deviation from the best fit spectrum does not exceed 1% for both species. Consequently, the corresponding uncertainty on the antiproton spectrum is smaller than the ones discussed in the next sections, and it will be neglected in the rest of this paper. The situation has significantly improved since Bottino & al. 1998, where an error of $\pm$ 25% was quoted.

3. Antiprotons production: secondary sources

Whereas p–p interactions are clearly the dominant process for secondary antiproton production in the galaxy, it has been realized long ago that p–nucleus and nucleus–nucleus collisions should also be taken into account (Gaisser & Schaefer 1992). They not only enhance the antiproton flux as a whole but also change its low energy tail, mostly for kinematical reasons. Unfortunately, very few experimental data are available on antiproton production cross-sections in nuclear collisions. A model-based evaluation is therefore necessary, and we chose to use the DTUNUC program. We first discuss sub-threshold antiproton production. Then we present the results of our calculations of above-threshold production, which we compare to experimental data and analytical formulæ.

3.1. p–p interaction

Antiproton production *via* the proton–proton interaction is the first reaction that one has to take into account in order to evaluate the $\bar{p}$ flux. So far, the Tan & Ng parameterization of $\bar{p}$ cross-section (Tan & Ng 1982, 1983) has been used by almost all studies on cosmic ray antiprotons. To be more precise, we recall the form of secondary contribution (*e.g.* eq. [A9], Appendix A.1)

$$q_{\bar{p}}^{sec}(r,E) \;=\; \int_{\rm Threshold}^{\infty} \frac{d\sigma}{dE}\left\{p(E') + H_{\rm ISM} \rightarrow \bar{p}(E)\right\}\, n_{He}\, \left\{4\,\pi\,\Phi_p(r,E')\right\}\, dE' \quad . \qquad (2)$$

Thus, in order to evaluate the secondary contribution of $p - H_{\rm ISM}$ reaction, we used the parameterization of Tan & Ng (1982, 1983). We refer the interested reader to the short discussion in Bottino et al. (1998) for further details, or to the source papers (Tan & Ng 1982, 1983) for a complete description. Finally, as an illustration, the impact of kinematics and threshold for the production rate can be found in Gaisser & Schaefer (1992).

3.2. Calculation of the differential cross-section of antiprotons production in p-He, He-p and He-He reactions

Some discrepancies between simple scalings of p–p cross-sections and experimental data on p–nucleus antiproton production cross-sections near threshold have been explained by taking into account internal nuclear Fermi motion (Shor et al. 1990). We first show that this effect does not change the cosmic antiproton spectrum. In such models, the momentum distribution is described by a double-gaussian function normalized to the total number of nucleons. The parameters are determined from scattering experiments (Moniz et al. 1971) and simple scaling laws. The cross-section results from a convolution

$$\frac{d^2\sigma_{p+nucleus\rightarrow\bar{p}+X}}{d\Omega dp} = \int d^3\mathbf{p_c} f(\mathbf{p_c}) \frac{d^2\sigma_{N+N\rightarrow\bar{p}+X}}{d\Omega dp}(E_{cm}) \;\; , \qquad (3)$$

where $\mathbf{p_c}$ is the internal nuclear momentum of the target nucleon, N denotes either a proton or a neutron (the model is isospin independent) and $\rm E_{cm}$ is the center of mass energy (with an off–shell target nucleon).

Near threshold, the nucleon–nucleon cross-section can be estimated from the transition matrix element and the available phase space by Fermi's golden rule. Using this simple approach with only one free parameter (namely the matrix element), fitted on data, we have been able to reproduce very well most experimental results available on subthreshold antiproton production. The kinematical term was computed using a Monte Carlo multi-particle

weighted event according to Lorentz-invariant Fermi phase space, whereas the integral was performed by adaptable gaussian quadrature. This method is not relevant to accurately determine the p–He, He–p or He–He cross-sections at any energy (as the momentum distribution becomes a δ function when the involved momenta are much greater than the Fermi momentum) but just to investigate their behaviour below the 6 GeV kinetic energy threshold. The main result is a very fast drop below the threshold. Even after convolution with the $\approx E^{-2.7}$ differential power law spectrum of primary cosmic rays, two orders of magnitude are lost in less than two GeV below the threshold. As a consequence, the subthreshold cross section can be neglected to compute the secondary antiprotons flux. The above-threshold discrepancies between data and simple models cannot be accounted for by this effect and a numerical Monte Carlo approach is necessary.

Following Simon et al. (1998), the Monte Carlo program DTUNUC[2] version 2.3 was therefore used to evaluate the cross-sections for p–He, He–p and He-He antiproton production reactions. The p–p reaction can be well accounted by the Tan & Ng parameterization (see previous section) whereas those involving nuclei heavier than helium are negligible due to cosmic abundances. This program is an implementation of the two-component Dual Parton Model (Capella et al. 1994) based on the Gribov-Glauber approach treating soft and hard scattering processes in a unified way. Soft processes are parameterized according to Regge phenomenology whereas lowest order perturbative QCD is used to simulate the hard component (Roesler 1997). This program calls PHOJET (Engel 1995) to treat individual hadron/nucleon/photon-nucleon interaction, PYTHIA (Sjöstrand 1994) for fragmentation of parton (according to the Lund model) and LEPTO ("Physics at HERA" 1992) for deep inelastic scattering off nuclei.

3.2.1. Comparison with experimental data

The resulting cross-sections have been compared with experimental data on proton–nucleus collisions. Figure 2 shows the differential cross-section of antiprotons production in p+C and p+Al collisions at 12 GeV laboratory kinetic energy recently measured at the Proton Synchrotron in the High Energy Accelerator Research Organisation (KEK–PS) for different antiprotons momenta (Sugaya et al. 1998). In most cases, measurements and DTUNUC simulations are compatible within uncertainties. The discrepancies are, anyway, taken into account in section 6.2 as uncertainties on the computed cross-sections. Figure 3 shows the invariant spectrum of antiprotons in p+Al collisions at 14.6 GeV/c laboratory momentum

[2]http://sroesler.home.cern.ch/sroesler/

as a function of $m_t - m$ where $m_t = \sqrt{p_t^2 + m^2}$ as obtained by experiment 802 at the Brookhaven Tandem Alternating Gradient Synchrotron (AGS) (Abbot et al. 1993). Data points have been normalized by using the inelastic cross-sections and plotted for a rapidity interval of $1.0 < y < 1.6$. The results of DTUNUC simulations are in perfect agreement with the measurements. This check is particularly important as it stands within the projectile energy range where most cosmic antiprotons are produced.

3.2.2. Comparison with analytical parameterization from Mokhov & Nikitin

Taking into account the qualitative predictions of the Regge phenomenology and partons model, Mokhov & Nikitin (1977) derived a parametrized inclusive cross-section for $p + A \rightarrow \bar{p} + X$:

$$\left(E\frac{d^3\sigma}{d^3p} \right)_{inv} = \sigma_{abs} C_1^{b(p_T)} (1 - x')^{C_2} \exp(-C_3 x') \Phi(p_T) \quad ,$$

$$\Phi(p_T) = \exp(-C_4 p_T^2) + C_5 \frac{\exp(-C_6 x_T)}{\left(p_T^2 + \mu^2\right)^4} \quad ,$$

where

$$b(p_T) = \begin{cases} b_o p_T \text{ if } p_T \leq \Gamma \quad ; \\ b_o \Gamma \text{ otherwise} \quad . \end{cases}$$

S is the invariant mass of system, p_T is the transverse momentum, $x_T \approx 2p_T/\sqrt{S}$, $x' = E^*/E^*_{max}$, E^* and E^*_{max} are the total energy of the inclusive particle in the center of mass frame and its maximum possible value. The parameters C_1 to C_6, b_0, μ^2 and Γ were not taken as given in Kalinovskii et al. (1989) but were re–fitted using an extensive set of experimental data leading to a better χ^2 (Huang 2001).

Contrary to experimental measurements that are only available for a small number of given energies, this analytical approach allows a useful comparison with DTUNUC cross-sections. The resulting spectrum has therefore been propagated using the model described in Section 4 and the results are in excellent agreement. The DTUNUC approach was nevertheless preferred since the Mokhov–Nikitin formula was fitted on rather heavy nuclei, and its use for p–He, He–p and He–He collisions would therefore require a substantial extrapolation.

3.2.3. Results for the antiprotons

The exclusive cross-section for antiproton production $d\sigma^{i,j}/dE_{\bar{p}}\,(E_{\bar{p}}, E_i)$, is obtained by multiplying the total inelastic cross-section of the considered reaction and the antiproton

multiplicity interaction given by DTUNUC.

This approach is time consuming since the cross-section is quite low and a large number of events must be generated to reach acceptable statistical uncertainties. The sampling points were chosen to be distributed on a logarithmic scale between 7 GeV (threshold) and 10 TeV per nucleon for the projectile nucleus and extrapolations rely on polynomial fits. The antiproton kinetic energy was varied from 0.1 GeV to 100 GeV. Figure 4 gives some examples of differential antiproton production cross-sections as obtained from DTUNUC.

4. Tertiary contribution

Once they have been created, antiprotons may interact with the interstellar material in three different ways. First, they may undergo elastic scatterings on galactic hydrogen. The cross-section for that reaction has been shown to peak in the forward direction (Eisenhandler 1976) so that the corresponding antiproton energy loss is negligible. Antiprotons are not perturbed by these elastic scatterings as they survive them while their energy does not change. They may also annihilate on interstellar protons. This process dominates at low energy, and its cross-section is given in Tan & Ng (1983). Last but not least, antiprotons may survive inelastic scatterings where the target proton is excited to a resonance. Antiprotons do not annihilate but lose a significant amount of their kinetic energy. Both annihilations and non–annihilating interactions contribute to the inelastic antiproton cross-section so that

$$\sigma^{\bar{p}p}_{non-ann} \;=\; \sigma^{\bar{p}p}_{ine} \;-\; \sigma^{\bar{p}p}_{ann} \quad , \tag{4}$$

where $\sigma^{\bar{p}p}_{ine}$ is parametrized as in Tan & Ng (1983).

For an antiproton kinetic energy $T_{\bar{\mathrm{p}}} \gtrsim 10$ GeV, the Tan & Ng parameterization of $\sigma^{\bar{p}p}_{ann}$ – which is based on experimental data – is no longer valid. The annihilation cross-section tends furthermore to be small at high energy. In any case, the antiproton inelastic but non–annihilating interaction cross section becomes equal to the total proton inelastic cross-section

$$\sigma^{\bar{p}p}_{non-ann} \equiv \sigma^{pp}_{ine} \quad . \tag{5}$$

The low and high energy relations for $\sigma^{\bar{p}p}_{non-ann}$ do match for an antiproton kinetic energy of $T_{\bar{\mathrm{p}}} = 13.3$ GeV.

The energy distribution of antiprotons that have undergone an inelastic but non–annihilating interaction has not been measured. It has been assumed here to be similar to the proton energy distribution after p–p inelastic scattering. An impinging antiproton

with kinetic energy $T'_{\bar{\rm p}}$ has then a differential probability of

$$\frac{dN_{\bar{p}}}{dE_{\bar{p}}} \;=\; \frac{1}{T'_{\bar{\rm p}}} \tag{6}$$

to end up with the final energy $E_{\bar{p}}$. That reaction leads to the flattening of their energy spectrum as the high–energy species of the peak that sits around a few GeV may replenish the low–energy part of the energy distribution. The corresponding source term for these so–called tertiary antiprotons may be expressed as

$$\begin{aligned} q_{\bar{p}}^{ter}(r,E_{\bar{p}}) \;&=\; \int_{E_{\bar{p}}}^{+\infty} \frac{d\sigma_{\bar{p}\,H\to\bar{p}\,X}}{dE_{\bar{p}}} \left\{E'_{\bar{p}} \to E_{\bar{p}}\right\}\, n_H\, v'_{\bar{p}}\, N^{\bar{p}}(r,E'_{\bar{p}})\, dE'_{\bar{p}} \\ &-\; \sigma_{\bar{p}\,H\to\bar{p}\,X}\left\{E_{\bar{p}}\right\}\, n_H\, v_{\bar{p}}\, N^{\bar{p}}(r,E_{\bar{p}}) \;\;. \end{aligned} \tag{7}$$

Since the differential cross-section is given by

$$\frac{d\sigma_{\bar{\rm p}\,{\rm H}\to\bar{\rm p}\,{\rm X}}}{dE_{\bar{\rm p}}} \;=\; \frac{\sigma^{\bar{p}p}_{non-ann}}{T'_{\bar{\rm p}}} \;\;, \tag{8}$$

the tertiary production term translates into

$$q_{\bar{p}}^{ter}(r,E) \;=\; 4\,\pi\, n_H \left\{ \int_E^{+\infty} \frac{\sigma^{\bar{p}p}_{non-ann}(E')}{T'}\, \Phi_{\bar{p}}(r,E')\, dE' \;-\; \sigma^{\bar{p}p}_{non-ann}(E)\, \Phi_{\bar{p}}(r,E) \right\} \;\;. \tag{9}$$

The integral over the antiproton energy E of $q_{\bar{p}}^{ter}(E)$ vanishes. This mechanism does not actually create new antiprotons. It merely redistributes them towards lower energies and tends therefore to flatten their spectrum. Notice in that respect that the secondary antiproton spectrum that results from the interaction of cosmic ray protons impinging on interstellar helium is already fairly flat below a few GeV. Since it contributes a large fraction to the final result, the effect under scrutiny here may not be as large as previously thought (Bergström et al. 1999).

As a matter of fact, antiprotons interact on both the hydrogen and helium of the Milky–Way ridge. Helium should also be taken into account in the discussion. As explained in Appendix (A.3), we have replaced the hydrogen density in relation (9) by the geometrical factor $n_H + 4^{2/3}\, n_{He}$ for the calculation of the tertiary component.

5. Propagation in a diffusion model

Propagation of cosmic rays can be studied within different theoretical frameworks, the most popular being the so-called Leaky Box model and the diffusion model. There is a

mathematical equivalence of these two approaches, which is valid only under special circumstances. In particular, they lead to different results for low grammages and for unstable cosmic ray species (see discussion in Maurin et al. 2001). Our preference for the diffusion model has several justifications. First, it is a more physical approach, in the sense that cosmic rays are believed to diffuse in the galactic disk and halo, which is in disagreement with the spatial homogeneity assumed in the Leaky Box. Second, the parameters entering the diffusion models are related to measurable physical quantities (at least in principle), like the galactic magnetic field, so that their value could be cross-checked with independent measurements. Finally, the diffusion approach is mandatory if one wants to take primary sources into account, as emphasized in the introduction.

The geometry of the problem used here is a classical cylindrical box (see for example Webber, Lee, & Gupta 1992) whose radial extension is $R = 20$ kpc, with a disk of thickness $2h = 200$ pc and a halo of half–height L lying in the interval $[1 - 15]$ kpc. Sources and interactions with matter are confined to the thin disk and diffusion which occurs throughout disc and halo with the same strength is independent of space coordinates. The solar system is located in the galactic disc ($z = 0$) and at a centrogalactic distance $R_\odot = 8$ kpc (Stanek & Garnavich 1998; Alves 2000). We emphasize that this model is exactly the one that has been used for the propagation of charged nuclei (Paper I) where it has been described in details. For the sake of completeness, we rewrite here the basic ingredients, and the parameters of the diffusion model we used.

5.1. The five parameters of the model

Our model takes into account the minimal known physical processes thought to be present during the propagation. Firstly, the diffusion coefficient $K(E)$

$$K(E) = K_0 \, \beta \times \mathcal{R}^\delta \tag{10}$$

where the normalisation K_0 is expressed in kpc^2 Myr^{-1} and δ is the spectral index ($\mathcal{R} = p/Z$ stands for the particle rigidity). Along with the spatial diffusion, one has the associated diffusion in energy space represented by a reacceleration term

$$K_{EE}(E) = \frac{2}{9} {V_a}^2 \frac{E^2 \beta^4}{K(E)} \quad . \tag{11}$$

Here K_{EE} stands for the energy diffusion coefficient which we evaluated in the no–recoil hard sphere scattering centers approximation. In particular V_a is the alfvénic speed of scatterers responsible of the energetic diffusion. Next, we allow a constant convective wind directed

outward in the z direction. This term is represented by the velocity V_c. Motivation of such forms for the various parameters has been given in Paper I and will not be repeated here. Last, we have to include effects of energy losses. Formulæ for the latter are those used for nuclei with the appropriated charge for an antiproton (see Paper I).

As a consequence, diffusion model is described with five parameters: the diffusion coefficient normalization K_0 and its power index δ, the convective galactic wind velocity V_c, the Alfvénic speed V_a, and finally the halo thickness L.

5.2. Configuration of the parameter space used for this analysis

The values of these parameters are needed to compute the propagated antiproton flux. They may be extracted from a careful analysis of charged cosmic ray nuclei data. This has been done in a previous study (Paper I), where all the sets of parameters consistent with B/C and sub–Fe/Fe data were determined. As the propagation history for all cosmic rays should be similar, this is thought to be a safe procedure. In this work, we used the same sets and the same numerical code to propagate antiprotons, to make sure our treatment is fully consistent with our previous work and that the results are consistent with nuclei data. This is in variance with previous works using diffusion models, where the propagation parameters were extracted from a leaky box analysis of nuclei. It should be noticed that some of the sets of parameters are probably disfavored by physical considerations. For instance, our models have Alfven velocities V_a ranging from 25 km s^{-1} to 85 km s^{-1}. The upper end of this range is too high. Indeed, the value of the galactic magnetic field ($B \approx 1 - 2$ μG, see for example Han & Qiao (1994) or Rand & Lyne (1994)) and the plasma density ($\langle n_e \rangle = 0.033$ cm^{-3} according to Nordgren, Cordes & Terzian (1992)) give 10 km s^{-1} $\lesssim V_a \lesssim$ 30 km s^{-1}. Besides, as mentionned in Paper I, the physical meaning of the value of V_a may depend on the assumptions made for the scattering process. A proportionality coefficient larger than 2/9 in relation (11) would imply smaller values for V_a. The following point should also be kept in mind: we considered that reacceleration only occured in the thin disk, *i.e.* in a zone of half-height $h_a = h = 100$ pc. If this process is efficient in a larger zone ($h_a > h$), the overall effect is unchanged provided that the Alfven velocity is scaled down to a lower value as $V_a \propto (L/h_a)^{1/2}$ (Seo & Ptuskin 1994). In our semi-analytical resolution of the diffusion model, the case $h_a \neq h$ cannot be straightforwardly taken into account, but the previous conclusion would still hold. Indeed, we can make the reacceleration zone larger by increasing the disk thickness h, while keeping constant the quantity $n_H h$ so that all the other effects are unaffected. For example, a $h_a = 1$ kpc reacceleration zone would lead to Alfven velocities about three times smaller so that in the sets of parameters used in this study, V_a would range

between ~ 10 km s^{-1} and ~ 30 km s^{-1}. Anyway, we adopt a conservative attitude and we do not apply any cut in our initial sets of parameters.

To sum up, we have applied all the configurations giving a good χ^2 (less than 40 for 26 data points and 5 parameters) in the B/C analysis of Paper I (see this paper for an extensive description of the nuclei analysis). We insist on the fact that none of this parameter is further modified or adjusted, they are not free parameters.

5.3. Calculation of the secondary component

Once the set of diffusion–propagation parameters is chosen as explained above, evaluation of the corresponding flux is straightforward. Semi–analytical solution for the antiproton background is given in Appendix A. Apart from the propagation, the two other necessary inputs are – as one can see from equation (A9) – the measured top of atmosphere H and He flux discussed in Section 2, and the nuclear processes described in Section 3 and 4.

To compare our results to experimental data, solar modulation (the effect of the solar wind on the interstellar flux crossing the heliosphere) must be taken into account. We chose to use the so-called force-field approximation, which is used in most antiproton studies (see last section for a discussion).

In all the subsequent results, the top–of–atmosphere antiproton flux has been obtained from the interstellar one with a modulation parameter of $\phi = 250$ MV ($\Phi \equiv Z/A \times \phi = 250$ MV), adapted for a period of minimal solar activity. This choice is motivated by the comparison to BESS data taken during the last solar minimum.

6. Results and uncertainties

6.1. Results

We have calculated the secondary, top–of–atmosphere antiproton spectrum obtained with the procedure described above. To begin with, we chose a particular set of diffusion parameters giving a good fit to the B/C data (see above). Namely, we have fixed: $K_0/L = 0.0345$ kpc^2 Myr^{-1}, $L = 9.5$ kpc, $V_c = 10.5$ km/s and $V_a = 85.1$ km/s. This set gives the best χ^2 for δ fixed to 0.6 and the resulting antiproton spectrum will be used as a reference in most subsequent figures. Fig. 5, displays this computed antiproton flux along with experimental data collected by the BESS spectrometer during two flights in a period of minimal solar activity. Circles correspond to the combined 1995 and 1997 data (Orito et al. 2000) and

squares to the 1998 ones (Maeno et al. 2000). The dotted lines represent the contribution to the total flux coming from the various nuclear reactions: from top to bottom are represented the contribution of p–p, p–He, He–p and He–He.

First of all, we notice that the calculated spectrum agrees very well with the BESS data points. This strong result gives confidence in our consistent treatment of nuclei and antiproton propagation. Second, even if the main production channel is the spallation of cosmic ray protons over interstellar hydrogen, we see that the contribution of protons over helium is very important, particularly at low energies (where a hypothetical primary signature would be expected). It emphasizes the necessity of having a good parameterization of the p–He reaction.

In the following sections, we study and quantify all the uncertainties and possible sources of errors in the secondary antiproton flux given above.

6.2. Uncertainties from diffusion parameters

The first source of uncertainty comes from the fact that the propagation parameters are not perfectly known, even if they are severely constrained by the analysis of B/C experimental results (Paper I). A quantitative estimate for this uncertainty is obtained by applying all the good parameter sets to antiproton propagation. In a first step, we set the diffusion coefficient spectral index δ to 0.6 and allow the four other parameters (K_0, L, V_c and V_a) to vary in the part of the parameter space giving a good fit to B/C. The resulting antiproton fluxes are presented in Fig. 6. The two curves represent the minimal and the maximal flux obtain with this set of parameters. In a second step, we also let δ vary in the allowed region of the parameter space, along with the four other parameters (Fig.7 and Fig.8 of Paper I). As before, the minimal and maximal fluxes are displayed in Fig. 7. The resulting scatter depends on the energy. More precisely, it is 9% from 100 MeV to 1 GeV, reaches a maximum of 24% at 10 GeV and decreases to 10% at 100 GeV. This gives our estimate of the uncertainties related to diffusion. They may be considered as quite conservative, as the range of allowed parameters could probably be further reduced by a thorough analysis of radioactive nuclei (Donato et al, in preparation) and also by new measurements of stable species.

6.3. Uncertainties from nuclear parameters

The uncertainties on the antiproton production cross-sections from p-He, He-p and He-He reactions have been evaluated using the most extensive set of experimental data

available. In addition to those described in Section 3.2.1, the average antiproton multiplicity in p–p collisions as measured by Antinucci et al. (1973) has also been checked out. Finally, measurements from Eichten et al. (1972) performed by the CERN-Rome group with the single-arm magnetic spectrometer (Allaby et al. 1971) were taken into account. They give the Lorentz invariant density (defined as $2E\delta^2\sigma/(\sigma_a p^2 \delta p \delta\Omega)$ where E and p are the laboratory energy and momentum of the produced antiproton and σ_a is the absorption cross-section) as a function of p and of the production angle θ. A wide range of values from $\theta = 17$ mrad to $\theta = 127$ mrad and from $p = 4$ GeV to $p = 16$ GeV has been explored.

All those measurements have been compared with DTUNUC results. As mentionned before, most of them are in excellent agreement with the simulation. The more important discrepancies were found for high-energy produced antiprotons in p-Be collisions and for low energy projectile protons in p-p collisions. This latter point is not surprising as the physical input of DTUNUC can hardly be justified for a center of mass energy $\sqrt{s} < 10$ GeV. In both cases, experimental cross-sections were lower than the simulated ones. Differences are never larger than a factor of two. To account for such effects we parameterized *maxima* and *mimina* cross-sections as a correction to the computed ones, depending on the projectile and antiproton energies. The simplest, *i.e.* linear, energy variation was assumed and the slope was chosen to be very conservative with respect to experimental data. Finally, it has been checked that changes in the Monte Carlo results induced by small variations of the input physical parameters remain within the previously computed errors.

According to Tan & Ng (1982, 1983), the uncertainty in the parameterization of their p–p cross-section should not exceed 10%. From another point of view, Simon et al. (1998) have compared two parameterization of the existing data along with the Monte Carlo model DTUNUC. They found large discrepancies which induce a 40% effect on the antiproton prediction. Nevertheless, since data are available for that reaction, we think that the Tan & Ng parameterization is more reliable than any Monte Carlo.

In Fig. 8 we present our estimation of the uncertainties related to nuclear physics. The central curve is our reference presented above. The upper one is obtained with the set of maximal p–He, He–p, He–He cross-sections while increasing the p–p cross-section by 10%. Similarly, the lower curve is obtained with the minimal values for these cross-sections while decreasing the p–p cross-section by 10%. Indeed, such a variation for p–p has been included for the sake of completeness even if it modifies the antiproton spectrum only by a few percents. As a conclusion, the shift of the upper and the lower curve with respect to the central one is of the order of 22–25 % over the energy range 0.1–100 GeV.

Besides these major sources of uncertainties, we have also investigated the influence of a possible error in the parameterization of the inelastic non–annihilating cross-section,

which gives rise to the tertiary component. We modified it by 20%, which is thought to be very conservative. We found that the antiproton spectrum is modified by less than 1%. In the same line of thought, the effect of total inelastic plus non-annihilating reactions on interstellar He is found to be negligible (see discussion in Appendix A.3).

6.4. Other uncertainties

There are few other sources of uncertainties. To begin with, as we discussed in Section 2, primary cosmic ray fluxes (protons and helium) have been measured with unprecedented accuracy. For the first time, the induced uncertainties on the antiproton spectrum can be neglected.

Next, the only parameters which have not been varied in the previous discussion are those related to the description of the interstellar medium, *i.e.* the densities $n_{\rm H}$ and $n_{\rm He}$. In all the preceding analysis, these were fixed to $n_{\rm ISM} \equiv n_{\rm H} + n_{\rm He} = 1$ cm^{-3} and $f_{\rm He} \equiv n_{\rm He}/n_{\rm ISM} = 10\%$ (same as in Paper I). We have tested the sensitivity of our results to changes in both $n_{\rm ISM}$ and $f_{\rm He}$. For this purpose, we found the new values for the diffusion parameters (for $\delta = 0.6$) giving a good fit to B/C, and applied them to antiprotons. Varying $f_{\rm He}$ in the range $5\% < f_{\rm He} < 15\%$, the resulting flux is modified by less than 15% over the whole energy range. Notice that this range of $f_{\rm He}$ values can be considered as very conservative (see discussion in Strong & Moskalenko 1998). A more realistic 10% error on $f_{\rm He}$ (i.e. $0.9\% < f_{\rm He} < 1.1\%$) would lead to a few % error on the antiproton spectrum. Alternatively, varying $n_{\rm ISM}$ from 0.8 to 1.2 cm^{-3}, the resulting flux is modified by less than 0.5% over the whole energy range. To sum up, the only contributing errors are from the helium fraction $f_{\rm He}$ through the dependence of antiproton production on corresponding cross-sections.

Finally, solar modulation induces some uncertainty. This problem is still debated, and a rigorous treatment of this effect is beyond the scope of this paper (see for example Bieber et al. 1999 for a recent analysis). However, in a "force-field" approximation, a general feature is that the steeper the spectrum, the greater the effect. Our antiproton spectra being rather flat, we do not expect them to be dramatically affected by a change in the modulation parameter. Anyway, this local effect is decorrelated from the propagation history. Solar modulation – which is the last energetic modification suffered by an incoming galactic cosmic ray – can thus be treated completely independently from the above analysis. Figure 9 shows our demodulated spectra together with other interstellar published spectra (Simon et al. 1998, Bieber et al. 1999, Moskalenko et al. 2001)

7. Conclusions

We have computed cosmic antiproton fluxes in the framework of a two-zone diffusion model taking into account galactic wind, stochastic reacceleration and energy losses. The propagation parameters have been chosen according to Maurin et al. (2001), as to be in agreement with cosmic ray nuclei data. The annihilating as well as the inelastic non-annihilating (tertiary) p–p reactions have been taken into account. The p–p, He–p, p–He and He–He nuclear reaction have also been included and the relevant cross-sections have been computed using the Monte Carlo program DTUNUC. The latest measured values for cosmic protons and helium fluxes from AMS and BESS have been considered.

The results may be summarized as follows. First, the values of all the inputs being either extracted from the analysis of nuclei (diffusion parameters δ, L, K_0, V_c and V_a) or measured (proton and helium fluxes), all the cosmic antiproton fluxes naturally coming out of the calculation are completely contained within the experimental error bars of BESS data.

The other strong conclusion is that all possible sources of uncertainties have been derived. They have been significantly improved with respect to the previous gross estimates.

In particular, those related to propagation range between 10% and 25%, depending on which part of the spectrum is considered, and those related to nuclear physics are below 25 %. We emphasize that the uncertainties related to propagation will probably be further reduced by a more complete study of cosmic ray nuclei, in particular by focusing on the radioactive species. We also note that more accurate data on cosmic ray nuclei fluxes would give better constraints on the diffusion parameters, which in turn would translate into lower uncertainties on antiprotons fluxes. The major remaining uncertainties come from nuclear physics and are already comparable to experimental error bars. As antiproton spectrum measurements should better in the near future, antiproton studies could be limited by nuclear undeterminacies. Further work and especially new measurements of antiproton production in the p–He channel would be of great interest.

Acknowledgments

We thank the anonymous second referee for useful comments on reacceleration. F.D. gratefully acknowledges a fellowship by the Istituto Nazionale di Fisica Nucleare. We also would like to thank the French Programme National de Cosmologie for its financial support. Finally, we are grateful to S. Roesler who provided us with DTUNUC and was very helpful in answering our questions.

A. Solution for the secondary antiprotons

We summarize in this annex the salient features of our derivation of the spallation antiproton energy spectrum. The propagation of cosmic–rays throughout the galaxy is described with a two–zone effective diffusion model which has been thoroughly discussed in a preceeding analysis (Paper I). The Milky–Way is pictured as a thin gaseous disk with radius $R = 20$ kpc and thickness $2h = 200$ pc where charged nuclei are accelerated and scatter on the interstellar gas to produce in particular secondary antiprotons. That thin ridge is sandwiched by two thick confinement layers. The effective diffusion of cosmic–rays throughout the galactic magnetic fields occurs uniformly within the disk and halo with the same strength. Furthermore, we consider here a constant wind V_c in the z direction. The associated adiabatic losses take place in the disk only.

A.1. High energy limit

As compared to the cosmic–ray nuclei on which the analysis of Paper I has focused, antiprotons have the same propagation history but differ as regards their production. The space–energy density $N^{\bar{p}}$ is related to the antiproton flux through

$$\Phi_{\bar{p}}(r, E) \;=\; \frac{1}{4\,\pi}\, v_{\bar{p}}(E)\, N^{\bar{p}}(r, E) \quad . \tag{A1}$$

As explained in Paper I – see in particular their equation (A1) – the density $N^{\bar{p}}$ satisfies the relation

$$\begin{aligned} 2\,h\,\delta(z)\, q_{\bar{p}}^{sec}(r, 0, E) \;&=\; 2\,h\,\delta(z)\,\Gamma_{\bar{p}}^{ine}\, N^{\bar{p}}(r, 0, E) \;+ \\ &+\; \left\{ V_c \frac{\partial}{\partial z} \;-\; K \left(\frac{\partial^2}{\partial z^2} + \frac{1}{r}\frac{\partial}{\partial r}\left(r \frac{\partial}{\partial r} \right) \right) \right\} N^{\bar{p}}(r, z, E) \quad , \end{aligned} \tag{A2}$$

as long as steady state holds. Diffusion and convection have been included. Inelastic interactions on interstellar atoms are described through the collision rate $\Gamma_{\bar{p}}^{ine}$ which will be discussed in more detail together with tertiary antiprotons. The antiproton density

$$N^{\bar{p}}(r, z, E) \;=\; \sum_{i=1}^{\infty} N_i^{\bar{p}}(z, E)\, J_0\left(\zeta_i \frac{r}{R} \right) \quad , \tag{A3}$$

and the secondary source term

$$q_{\bar{p}}^{sec}(r, 0, E) \;=\; \sum_{i=1}^{\infty} q_{\bar{p}\,i}^{sec}(E)\, J_0\left(\zeta_i \frac{r}{R} \right) \quad , \tag{A4}$$

may be expanded over the orthogonal set of Bessel functions $J_0(\zeta_i x)$ where ζ_i stands for the ith zero of J_0 while $i = 1 \ldots \infty$. The boundary condition $N^{\bar{p}} \equiv 0$ is therefore readily ensured for $r = R$. The Bessel transform of the antiproton density has vertical dependence

$$N_i^{\bar{p}}(z,E) \;=\; N_i^{\bar{p}}(E)\;\exp\left\{\frac{V_c\,z}{2\,K}\right\}\;\left\{\sinh\left\{\frac{S_i}{2}\;(L-z)\right\}/\sinh\left\{\frac{S_i}{2}\,L\right\}\right\}\quad , \tag{A5}$$

where the quantity S_i is defined as

$$S_i \equiv \left\{\frac{V_c^2}{K^2}\;+\;4\frac{\zeta_i^2}{R^2}\right\}^{1/2}\quad . \tag{A6}$$

Solving equation (A2) with the help of the Bessel expansions (A3) and (A4) leads to the simple relation

$$N_i^{\bar{p}}(E) \;=\; \frac{2\,h}{A_i^{\bar{p}}}\;q_{\bar{p}\,i}^{sec}(E)\quad , \tag{A7}$$

that mostly holds at high energy – say above ~ 100 GeV – where energy losses and diffusive reacceleration do not play any major role. The coefficients $A_i^{\bar{p}}$ are given by

$$A_i^{\bar{p}}(E) \equiv 2\,h\,\Gamma_{\bar{p}}^{ine}\;+\;V_c\;+\;K\,S_i\coth\left\{\frac{S_i L}{2}\right\}\quad . \tag{A8}$$

Notice that the diffusion coefficient K – that comes into play in the definition of S_i and therefore of $A_i^{\bar{p}}$ – essentially depends on the rigidity. One should keep in mind that the relationship between K and the energy per nucleon may actually depend on the nuclear species at stake through the average charge per nucleon Z/A.

Secondary antiprotons are produced by the spallation reactions of high–energy cosmic–ray protons and helium on the interstellar material of the Milky Way ridge at $z = 0$. The source term

$$q_{\bar{p}}^{sec}(r,E) \;=\; \int_{\rm Threshold}^{\infty}\frac{d\sigma}{dE}\left\{a(E')+b\rightarrow\bar{p}(E)\right\}\;n_b\;\left\{4\,\pi\,\Phi_a(r,E')\right\}\;dE' \tag{A9}$$

corresponds to particles a – protons or helium – impinging on atoms b – hydrogen or helium – at rest. Four different production channels need therefore to be considered depending on the nature of the cosmic–rays and of the stellar gas. Proton–proton collisions are discussed in Section (3.1) whereas interactions that involve at least a helium nucleus are reviewed in Section (3.2). Bessel expanding relation (A9) leads to

$$q_{\bar{p}\,i}^{sec}(E) \;=\; \int_{\rm Threshold}^{\infty}\frac{d\sigma}{dE}\left\{a(E')+b\rightarrow\bar{p}(E)\right\}\;n_b\,v'\,N_i^a(E')\,dE'\quad . \tag{A10}$$

The primary species a are accelerated in the galactic disk so that their own production rate may be expressed as

$$q_a\,(r,z,E) \;=\; 2\,h\,\delta(z)\,q_a\,(r,0,E) \propto q_a^{tot}(E)\,f(r)\quad , \tag{A11}$$

where $q_a^{tot}(E)$ denotes the global galactic production rate of particles – protons or helium – with energy E in the energy bin dE. We have assumed here that the energy dependence of that production rate could be disentangled from its distribution $f(r)$ along the galactic disk. The bulk of the secondary antiproton production takes place for a typical energy of the impinging species of $E \sim 20 - 30$ GeV/n. Note also that the primary fluxes $\Phi_a(E)$ are monotonically decreasing with the energy E. Both energy losses and diffusive reacceleration have therefore a negligible effect on the spectra Φ_a. We readily infer that the Bessel transform N_i^a may be expressed as

$$N_i^a(E) \; = \; \frac{q_i}{A_i^a} \, q_a^{tot}(E) \;\; , \tag{A12}$$

where the coefficients A_i^a are given by a relation similar to (A8) whereas the quantities q_i are defined as

$$q_i \; = \; \frac{1}{\pi R^2} \, \frac{1}{J_1^2\left(\zeta_i\right)} \, \left\{ \int_0^1 u \, du \, J_0\left\{\zeta_i u\right\} \, f\left\{r = uR\right\} \right\} \, \left\{ \int_0^1 u \, du \, f\left\{r = uR\right\} \right\}^{-1} \;\; . \tag{A13}$$

The cosmic–ray flux Φ_a may be determined everywhere as it is related to the Bessel transform N_i^a through relations similar to (A1) and (A3). The cosmic–ray flux Φ_a scales in particular with the global galactic production rate q_a^{tot}. This allows to determine the latter by imposing that the interstellar proton and helium fluxes at the solar system do actually match the observations.

A.2. Full solution without tertiaries

Forgetting for a while that the inelastic collisions of antiprotons with the interstellar gas may be disentangled into annihilating and non–annihilating interactions, we have to modify relation (A2) so as to take into account now the energy losses as well as diffusive reacceleration. This is straightforward since those processes take place only in the disk and not in the halo. Once again, following the procedure described in Paper I, one gets the differential equation

$$A_i^{\bar{p}} \, N_i^{\bar{p}} \; + \; 2\,h\,\partial_E \left\{ b_{loss}^{\bar{p}}(E) \, N_i^{\bar{p}} \; - \; K_{EE}^{\bar{p}}(E) \, \partial_E N_i^{\bar{p}} \right\} \; = \; 2\,h\,q_{\bar{p}\,i}^{sec}(E) \;\; , \tag{A14}$$

where $b_{loss}^{\bar{p}}$ and $K_{EE}^{\bar{p}}$ stand respectively for the energy losses and the diffusion in energy.

A.3. Full solution with tertiaries

We have seen that the source term for tertiaries is

$$q_{\bar{p}}^{ter}(r,E) \; = \; 4\,\pi\,n_H \left\{ \int_E^{+\infty} \frac{\sigma_{non-ann}^{\bar{p}p}(E')}{T'} \, \Phi_{\bar{p}}(r,E') \, dE' \; - \; \sigma_{non-ann}^{\bar{p}p}(E) \, \Phi_{\bar{p}}(r,E) \right\} \;\; . \tag{A15}$$

Remembering that the antiproton flux $\Phi_{\bar{p}}$ is related to the space–energy density $N^{\bar{p}}$ through equation (A1) and Bessel expanding relation (A15) leads to

$$q^{ter}_{\bar{p}\,i}(E) \;=\; \int_E^{+\infty} \frac{\sigma^{\bar{p}p}_{non-ann}(E')}{T'}\, n_H\, v'\, N^{\bar{p}}_i(E')\, dE' \;-\; \sigma^{\bar{p}p}_{non-ann}(E)\, n_H\, v\, N^{\bar{p}}_i(E) \quad . \tag{A16}$$

In the thin disk approximation, that expression needs to be multiplied by $2\,h\,\delta(z)$. The Bessel transforms $N^{\bar{p}}_i(z=0,E)$ of the antiproton density obey now the integro–differential equation

$$A^{\bar{p}}_i\, N^{\bar{p}}_i \;+\; 2\,h\,\partial_E \left\{ b^{\bar{p}}_{loss}(E)\, N^{\bar{p}}_i \;-\; K^{\bar{p}}_{EE}(E)\, \partial_E N^{\bar{p}}_i \right\} \;=\; 2\,h\, \left\{ q^{sec}_{\bar{p}\,i}(E) + q^{ter}_{\bar{p}\,i}(E) \right\} \quad . \tag{A17}$$

Notice that in the definition of the coefficients $A^{\bar{p}}_i$, the rate $\Gamma^{ine}_{\bar{p}}$ should now be replaced by

$$\Gamma^{ann}_{\bar{p}}(E) \;=\; \sigma^{\bar{p}p}_{ann}(E)\, v_{\bar{p}}(E)\, n_H \quad , \tag{A18}$$

where annihilations alone are considered. The inelastic non–annihilating reactions are directly dealt with in the tertiary production term $q^{ter}_{\bar{p}\,i}$.

Helium should also be taken into account in our discussion of the annihilations as well as of the inelastic but non–annihilating interactions which antiprotons undergo with interstellar matter. As there are no measurements, we have adopted as an educated guess the geometrical approximation which consists in scaling the appropriate cross-sections by a factor of $4^{2/3}$ when we deal with helium. In the formulæ (A16), (A16) and (A18), we have therefore replaced the hydrogen density n_H by $(n_H + 4^{2/3}\, n_H e)$. Such a replacement has little effect. That overall change in the propagated antiproton spectrum is at most 1%.

B. Numerical resolution

We need now to solve the energy–diffusion equation (A17) for each Bessel order i. In the absence of diffusive reacceleration and energy losses, its solution $N^{\bar{p}\,0}_i$ satisfies the relation

$$A^{\bar{p}}_i\, N^{\bar{p}\,0}_i \;=\; 2\,h\, \left\{ q^{sec}_{\bar{p}\,i}(E) + q^{ter}_{\bar{p}\,i}(E) \right\} \quad . \tag{B1}$$

Defining the functions

$$\mathcal{C}(E) \;=\; \frac{2\,h}{A^{\bar{p}}_i\, T} \quad , \tag{B2}$$

and

$$a(E) \;=\; \frac{K^{\bar{p}}_{EE}(E)}{T} \quad , \tag{B3}$$

where $T = E_{\bar{p}} - m_{\bar{p}}$ is the antiproton kinetic energy, allows us to simplify equation (A17) into

$$u \; + \; \mathcal{C} \, \frac{d}{dx} \left\{ b_{loss}^{\bar{p}} \, u \; - \; a \, \frac{du}{dx} \right\} \; = \; u^0 \quad , \tag{B4}$$

where u^0 and u respectively stand for $N_i^{\bar{p}\,0}$ and $N_i^{\bar{p}}$. We can express relation (B4) on a one–dimensional grid extending from $x_{\rm inf}$ to $x_{\rm sup}$ with $x = \ln (T/T_{\rm inf})$. We are interested in kinetic energies extending from $T_{\rm inf} = 100$ MeV up to $T_{\rm sup} = 100$ GeV. The spacing between two points in energy is

$$\Delta x \; = \; \frac{1}{N} \, \ln \left\{ \frac{T_{\rm max}}{T_{\rm min}} \right\} \quad , \tag{B5}$$

where N has been fixed to 150 in our code. Our resolution method lies on the direct inversion of the algebraic linear equations that translate relation (B4) on the set of the $N+1$ different values of the variable x. If j denotes the point at position

$$x_j \; = \; \frac{j}{N} \, \ln \left\{ \frac{T_{\rm max}}{T_{\rm min}} \right\} \quad , \tag{B6}$$

we get

$$u_j^0 \; = \; A_{j,j-1} \, u_{j-1} \; + \; A_{j,j} \, u_j \; + \; A_{j,j+1} \, u_{j+1} \quad . \tag{B7}$$

The matrix A that connects u to u^0 has been written here so as to be tridiagonal. This allows for a fast inversion of the algebraic equation (B7).

• For $0 < j < N$, the tridiagonal matrix A may be written as

$$a_j \; = \; A_{j,j-1} \; = \; - \, \frac{\mathcal{C}_j}{2 \, \Delta x} \, b_{j-1}^{\rm ion} \; - \; \frac{\mathcal{C}_j}{\Delta x^2} \, a_{j-1/2} \quad , \tag{B8}$$

while

$$b_j \; = \; A_{j,j} \; = \; 1 \; + \; \frac{\mathcal{C}_j}{\Delta x^2} \, \left(a_{j-1/2} + a_{j+1/2} \right) \quad , \tag{B9}$$

and

$$c_j \; = \; A_{j,j+1} \; = \; \frac{\mathcal{C}_j}{2 \, \Delta x} \, b_{j+1}^{\rm ion} \; - \; \frac{\mathcal{C}_j}{\Delta x^2} \, a_{j+1/2} \quad , \tag{B10}$$

• The boundary $j = 0$ corresponds to the low energy tip $T_{\rm min} = 100$ MeV where we have implemented the condition $\ddot{u}(x_{\rm min}) = 0$. This translates into $\dot{u}_{-1/2} = \dot{u}_{1/2}$ and leads to the matrix elements

$$a_0 \; = \; A_{0,-1} \; = \; 0 \quad , \tag{B11}$$

and

$$b_0 \; = \; A_{0,0} \; = \; 1 \; - \; \frac{\mathcal{C}_0}{\Delta x} \, b_0^{\rm ion} \; + \; \frac{\mathcal{C}_0}{\Delta x^2} \, \left(a_{1/2} - a_{-1/2} \right) \quad , \tag{B12}$$

and also

$$c_0 \;=\; A_{0,1} \;=\; \frac{\mathcal{C}_0}{\Delta x}\, b_1^{\rm ion} \;-\; \frac{\mathcal{C}_0}{{\Delta x}^2}\, \left(a_{1/2} - a_{-1/2} \right) \quad . \tag{B13}$$

• We have finally assumed that both u and u^0 were equal at the high–energy boundary $j = N$. In this regime, the energy losses and the diffusive reacceleration should not affect too much the cosmic–ray energy spectrum. This translates into the simple conditions

$$a_N \;=\; A_{N,N-1} \;=\; 0 \quad , \tag{B14}$$

and

$$b_N \;=\; A_{N,N} \;=\; 1 \quad , \tag{B15}$$

whereas, by definition

$$c_N \;=\; A_{N,N+1} \;=\; 0 \quad . \tag{B16}$$

Inverting a tridiagonal matrix such as A may be potentially dangerous as Jordan pivoting is not implemented in the standard resolution scheme. As a matter of fact, energy losses and diffusive reacceleration lead to a moderate change in the antiproton spectrum. This translates into the fact that the matrix A is close to unity. We have nevertheless checked that our results remained unchanged when Gauss–Jordan inversion was used (Press et al. 1992). We have also modified relation (B4) into the time–dependent equation

$$\frac{\partial u}{\partial t} \;+\; u \;+\; \mathcal{C}\, \frac{d}{dx} \left\{ b_{loss}^{\bar{p}}\, u \;-\; a\, \frac{du}{dx} \right\} \;=\; 0 \quad . \tag{B17}$$

It may be shown that the static solution u to equation (B4) also obtains from the superposition

$$u \;=\; \int_0^{+\infty} u^{burst}(t)\; dt \quad , \tag{B18}$$

of the reaction $u^{burst}(t)$ to an initial burst

$$u^{burst}(0) \;=\; u^0 \tag{B19}$$

taking place at $t = 0$ and subsequently evolving according to relation (B17). The later equation has also been solved on a discrete set of $N + 1$ values of the antiproton kinetic energy while a Crank–Nicholson scheme was implemented. Once again, the result (B18) is the same as what the direct inversion of the algebraic set of relations (B7) gives. We are therefore confident that our resolution procedure is robust.

The tertiary source term depends on the global antiproton energy spectrum that is itself determined by the differential equation (A17). Starting from a trial antiproton spectrum –

say for instance $N_i^{\bar{p}\,0}$ with only the secondary production mechanism $q_{\bar{p}\,i}^{sec}(E)$ cranked up – we invert equation (B7). The new energy spectrum is used to compute the tertiary source term $q_{\bar{p}\,i}^{ter}(E)$ through the integral (A16). We may therefore proceed once again through the same steps and invert the diffusive reacceleration equation (A17) until the antiproton spectrum becomes stable. We have actually checked that convergence obtains after ~ 5 recursions.

REFERENCES

Abbott, T., et al. 1993, Phys. Rev. C, 47, 1351

AMS Collaboration Alcaraz J., et al. 2000a, Phys. Lett. B, 472, 215;
——. 2000b, Phys. Lett. B, 490, 27;
——. 2000c, Phys. Lett. B, 494, 193.

Allaby, J.V., et al. 1971, Phys. Lett. B, 34, 431

Alves, D.R. 2000, ApJ, 539, 732

Antinucci, M., et al. 1973, Lett. Nuovo Cimento, 6, 121

Bergström, L., Edsjö, J., & Ullio, P. 1999, ApJ, 526, 215

Bieber, J. W., et al. 1999, Phys. Rev. Lett., 83, 674

Bottino, A., Favero, C., Fornengo, N., & Mignola, G. 1995, Astropart. Physics, 3, 77

Bottino, A., Donato, F., Fornengo, N., & Salati, P. 1998, Phys. Rev. D, 58, 123503

Capella, A., Sukhatme, U., Tan, C.-I., & Tran Thanh Van, J. 1994, Phys. Rept., 236, 225

Chardonnet, P., Mignola, G., Salati, P., & Taillet, R. 1996, Phys. Lett. B, 384, 161

Eichten, T., et al. 1972, Nucl. Phys., 44, 333

Eisenhandler, E., et al. 1976, Nucl. Phys. B, 113, 1

Ellis.J, Flores, R.A., Freese, K., Ritz, S., Seckel, D., & Silk, J. 1988, Phys. Lett. B, 214, 403

Engel, R. 1995, Z. Phys. C, 66, 203

Gaisser, T.K., & Schaefer, R.K. 1992, ApJ, 395, 174

Halm, I., Jansen, F., & de Niem, D. 1993, A&A, 269, 601

Han, J.L, & Qiao, G.J., 1994, A&A, 288, 759.

Huang, C.Y., PhD thesis, Grenoble-I University, to be defended (2001)

Kalinovskii, A.N., Mokhov, N.V., & Nikitin, Yu.P. 1989, AIP, New-York

Lagage, P.O., & Cesarsky, C.J. 1985, A&A, 147, 127

Maeno, T., et al., astro–ph/0010381

Maurin, D., Donato, F., Taillet, R., & Salati, P. 2001, ApJ, 555, 585 (Paper I)

Mitsui, T., Maki, K., & Orito, S. 1996, Phys. Lett. B, 389, 169

Mokhov, N.V., Nikitin, & Yu.P. 1977, Nuclear Physics and Cosmic Rays (6th ed.; State University, Khar'kov)

Moniz, E., et al. 1971, Phys. Rev. Lett., 26, 445

Moskalenko, I.V., Strong, A.W., & Reimer, O. 1998, A&A, 338, L75

Moskalenko, I.V., Strong, A.W., Ormes, J.F., Potgieter, M.S., 2001, astro–ph/0106567

Nordgren, T.E, Cordes, J.M, & Terzian, Y. 1992, AJ, 104, 1465

Orito, S., et al. 2000, Phys. Rev. Lett., 84, 1078

1992, Physics at HERA, Vol.3, ed. W. Buchmueller & G.Ingelman (DESY Hamburg), 1366

Press, W.H., Teukolsky, S.A, Vetterling, W.T., & Flannery, B.P, 1992, Numerical Recipes in C – The Art of Scientific Computing (2d ed.; Cambridge University Press)

Rand, R.J., & Lyne, A.G. 1994, MNRAS, 268, 197

Roesler, R. 1997, PhD thesis, University Gesamthochschule Siegen

Rudaz, S., & Stecker, F.W. 1988, ApJ, 325, 16

Sanuki, T., et al. 2000, ApJ, 545, 1135

Seo, E.S., & Ptuskin, V.S. 1994, ApJ, 431, 705

Shor, A., et al. 1990, Nucl. Phys. A, 514, 717

Silk, J., & Srednicki, M. 1984, Phys. Rev. Lett., 53, 624

Simon, M., & Heinbach, U. 1996, ApJ, 456, 519

Simon, M., Molnar, A., & Roesler, S. 1998, ApJ, 499, 250

Sjöstrand, T. 1994, Compt. Phys. Comm., 82, 75

Stanek, K.Z., & Garnavich, P.M. 1998, ApJ, 503, L131

Starkman, G.D., & Vachaspati, T. 1996, Phys. Rev. D, 53, R6711

Stephens, S.A., & Golden, R.L. 1988, A&A, 202, 1

Strong, A.W., & Moskalenko, I.V. 1998, ApJ, 509, 212

Sugaya, Y., et al. 1998, Nucl. Phys. A, 634, 115

Tan, L.C., & Ng, L.K. 1982, Phys.Rev.D, 26, 1179

Tan, L.C., & Ng, L.K. 1983, J. Phys. G: Nucl.Phys, 9, 227

Webber, W.R., Lee, M.A., & Gupta, M. 1992, ApJ, 390, 96

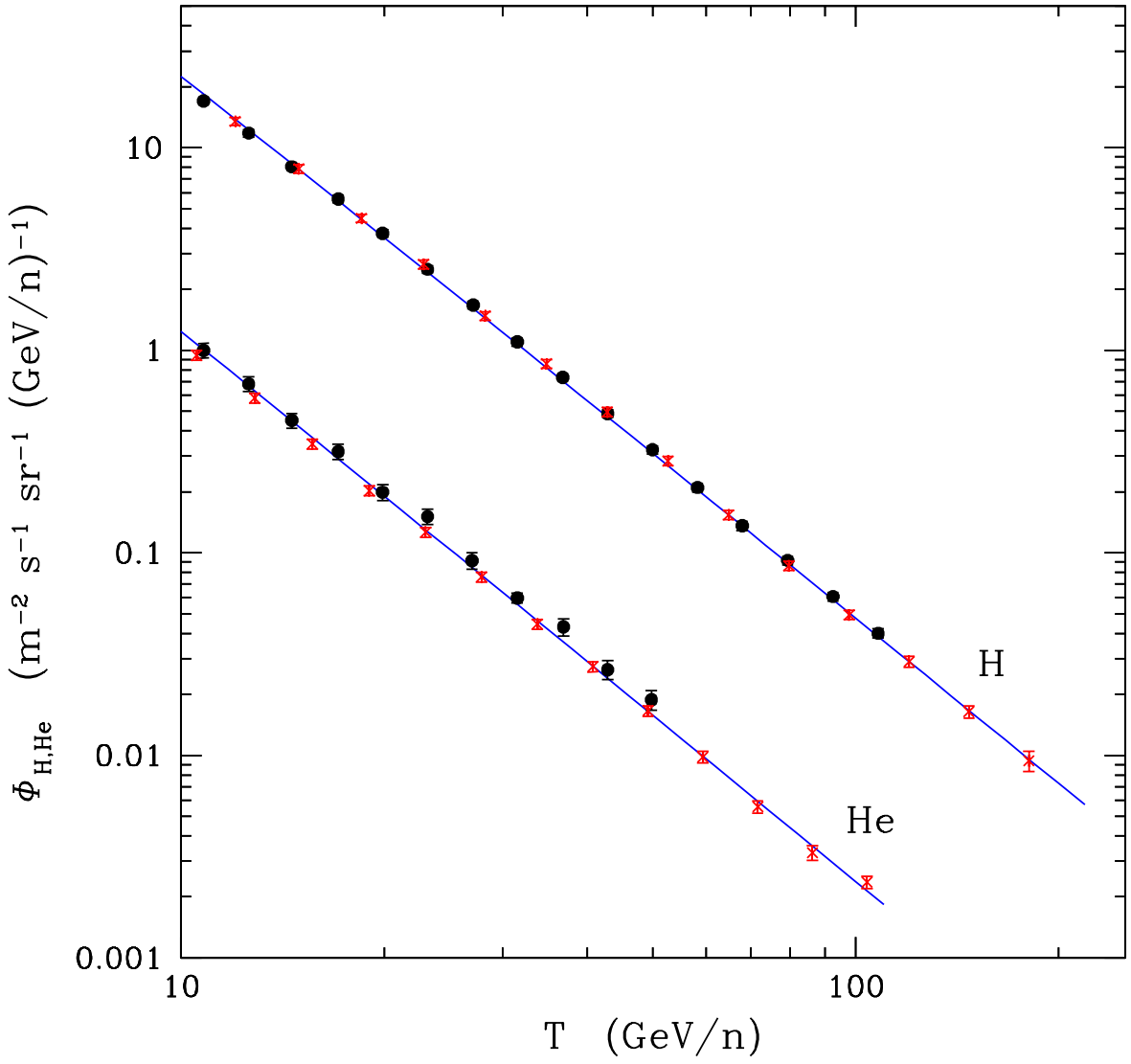

Fig. 1.— The upper (lower) curve displays the measured proton (helium) flux along with an analytical fit (see text). On both curves, data are from AMS (Alcaraz et al. 2000a, 2000b, 2000c) (crosses) and BESS (Sanuki et al. 2000) (filled circles).

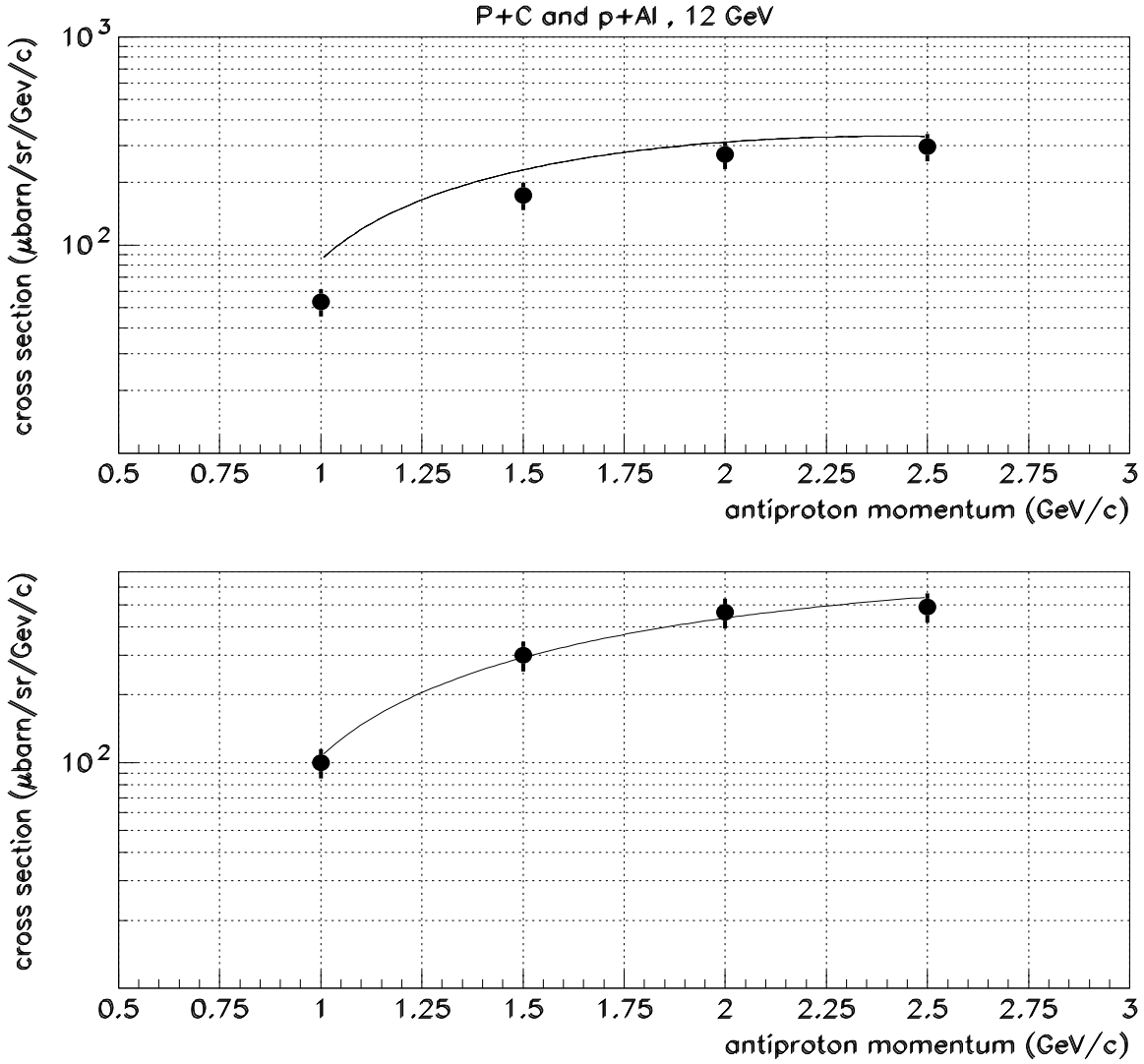

Fig. 2.— Here are displayed the antiproton production cross-section in p+C (top) and p+Al (bottom) collisions at 12 GeV laboratory kinetic energy. Filled circles are experimental data (Sugaya et al. 1998) and the lines are from our DTUNUC simulations. The error bars have been assumed to be 15%. This value is usual for such experiments and was suggested by a χ^2 analysis combining most data available.

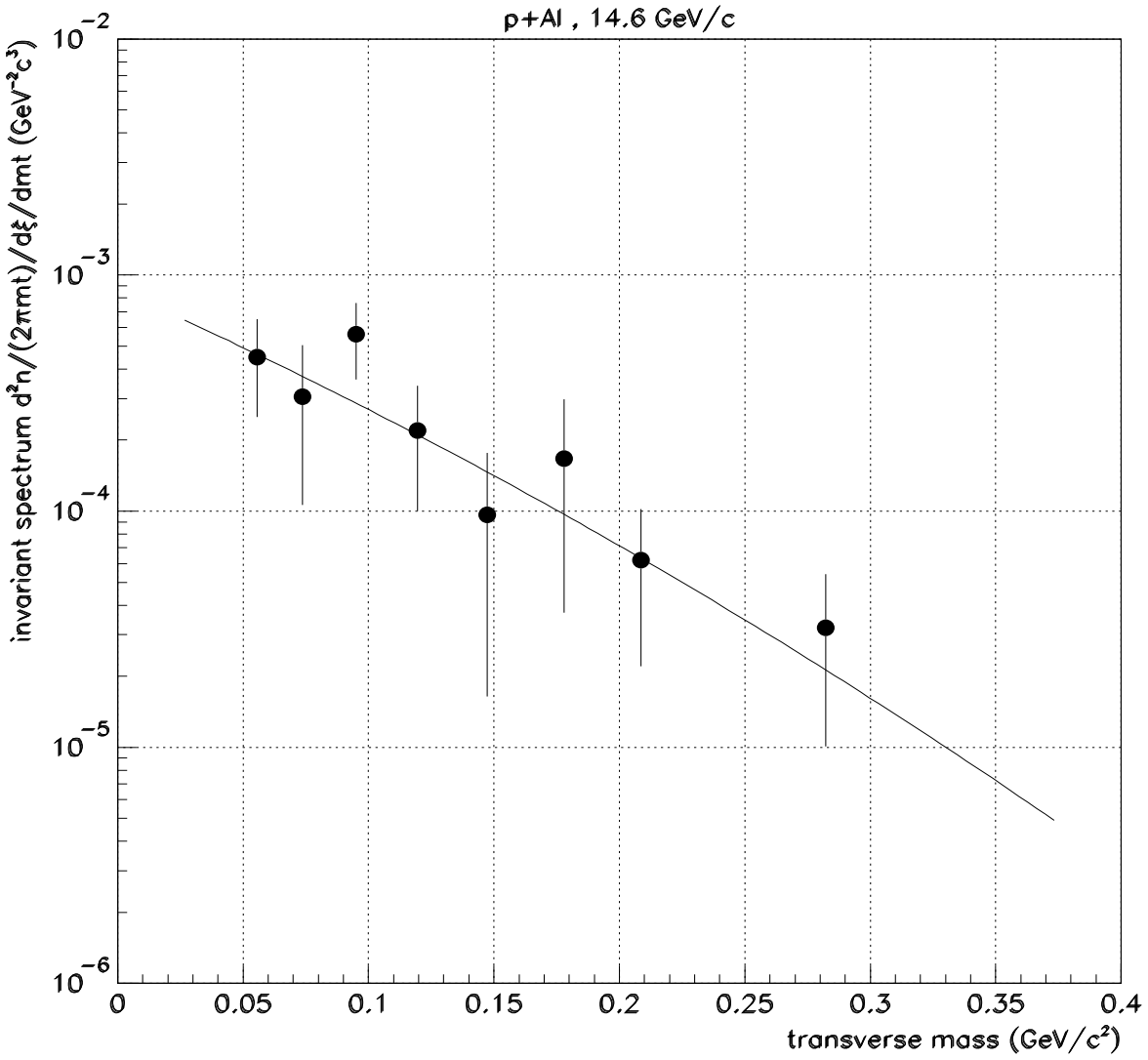

Fig. 3.— Invariant spectrum of $\bar{p}$ in p+Al collisions at 14.6 GeV laboratory momentum. Filled circles are experimental data (Abbott et al. 1993) and the line is from our DTUNUC simulation.

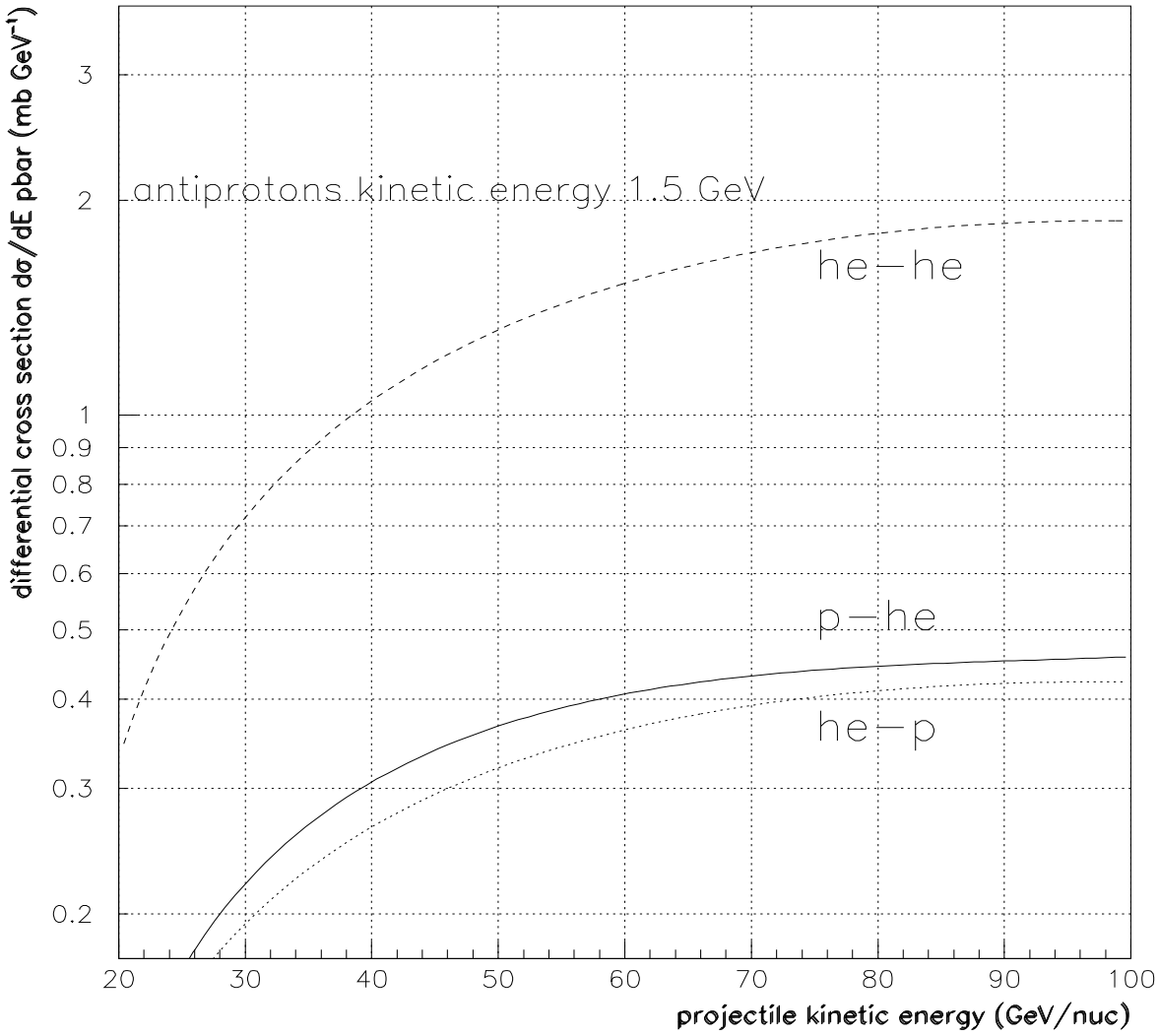

Fig. 4.— From top to bottom: antiproton differential production cross-section in He–He, p–He and He–p reactions for antiprotons kinetic energy 1.5 GeV, as obtained with DTUNUC simulations.

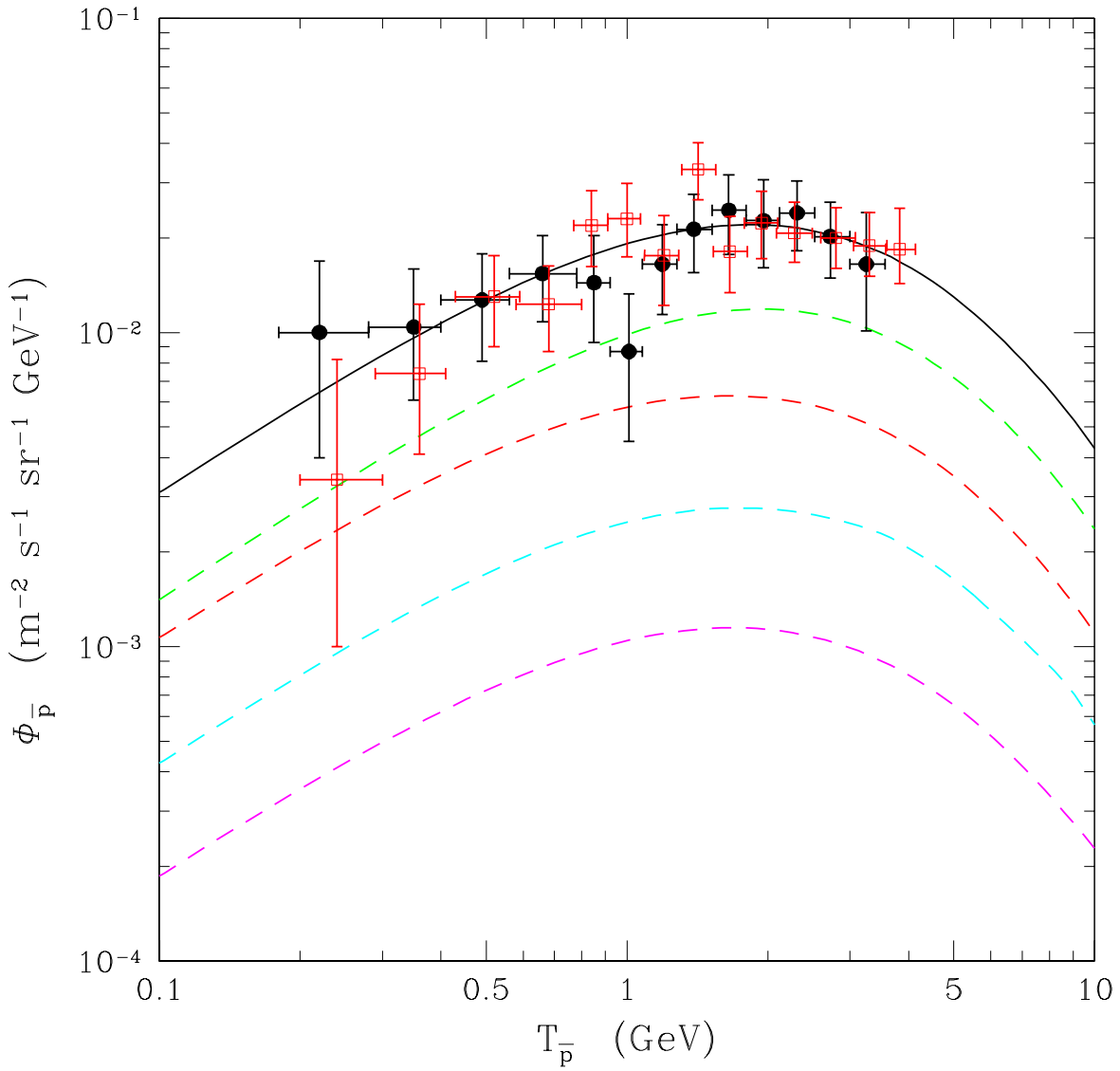

Fig. 5.— Solid line shows the total top-of-atmosphere (TOA) secondary antiproton spectrum for the reference set of diffusion parameters (see text for details). Dashed lines are the contributions to this total flux from various nuclear reactions (from top to bottom: p–p, p–He, He–p and He–He). Data points are taken from BESS 95+97 (filled circles) and from BESS 98 (empty squares).

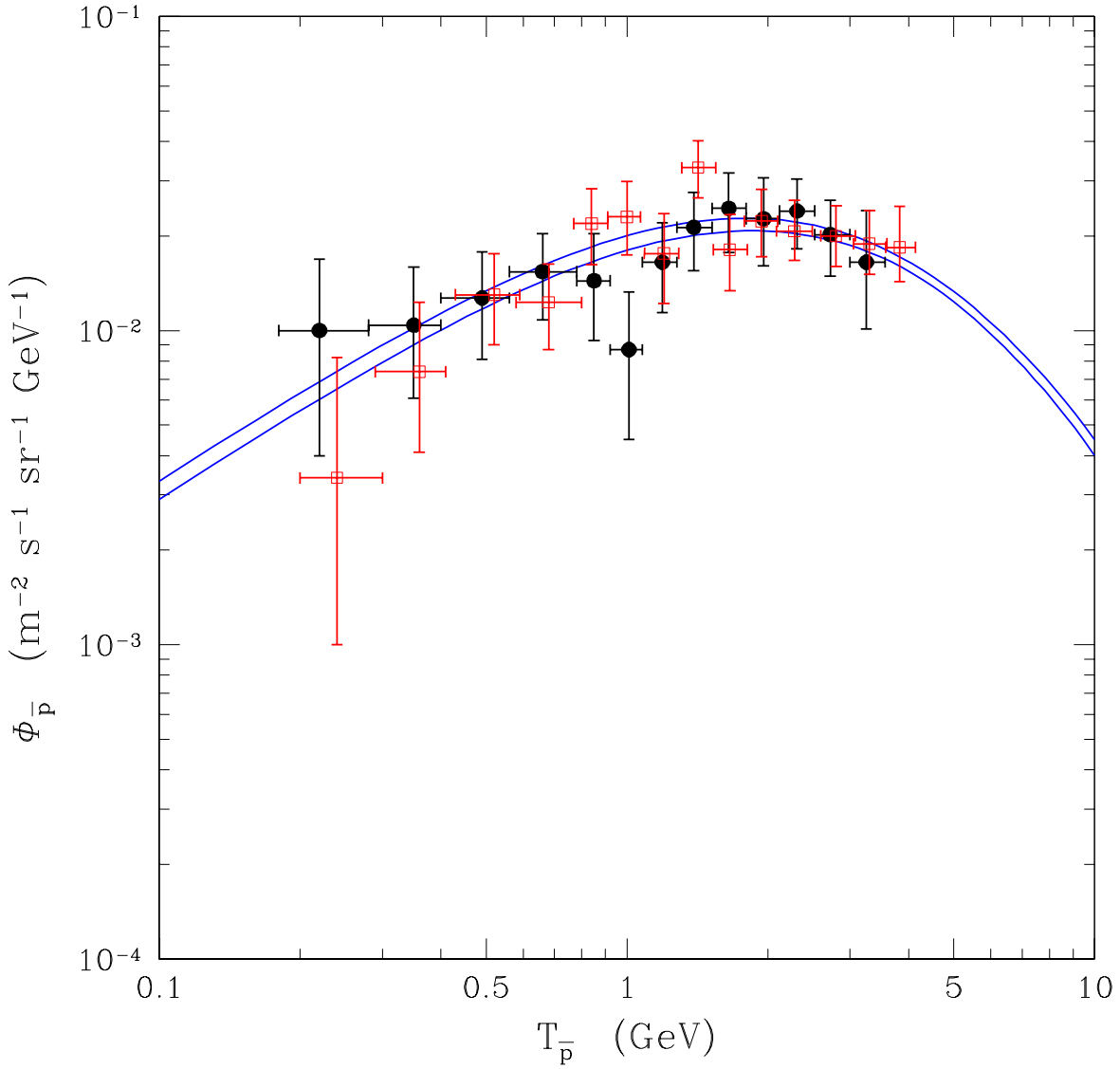

Fig. 6.— This plot shows the envelope of the TOA antiproton spectra generated with the sets of diffusion parameters consistent with B/C and for which δ has been fixed to 0.6 (data points are the same as in Fig. 5).

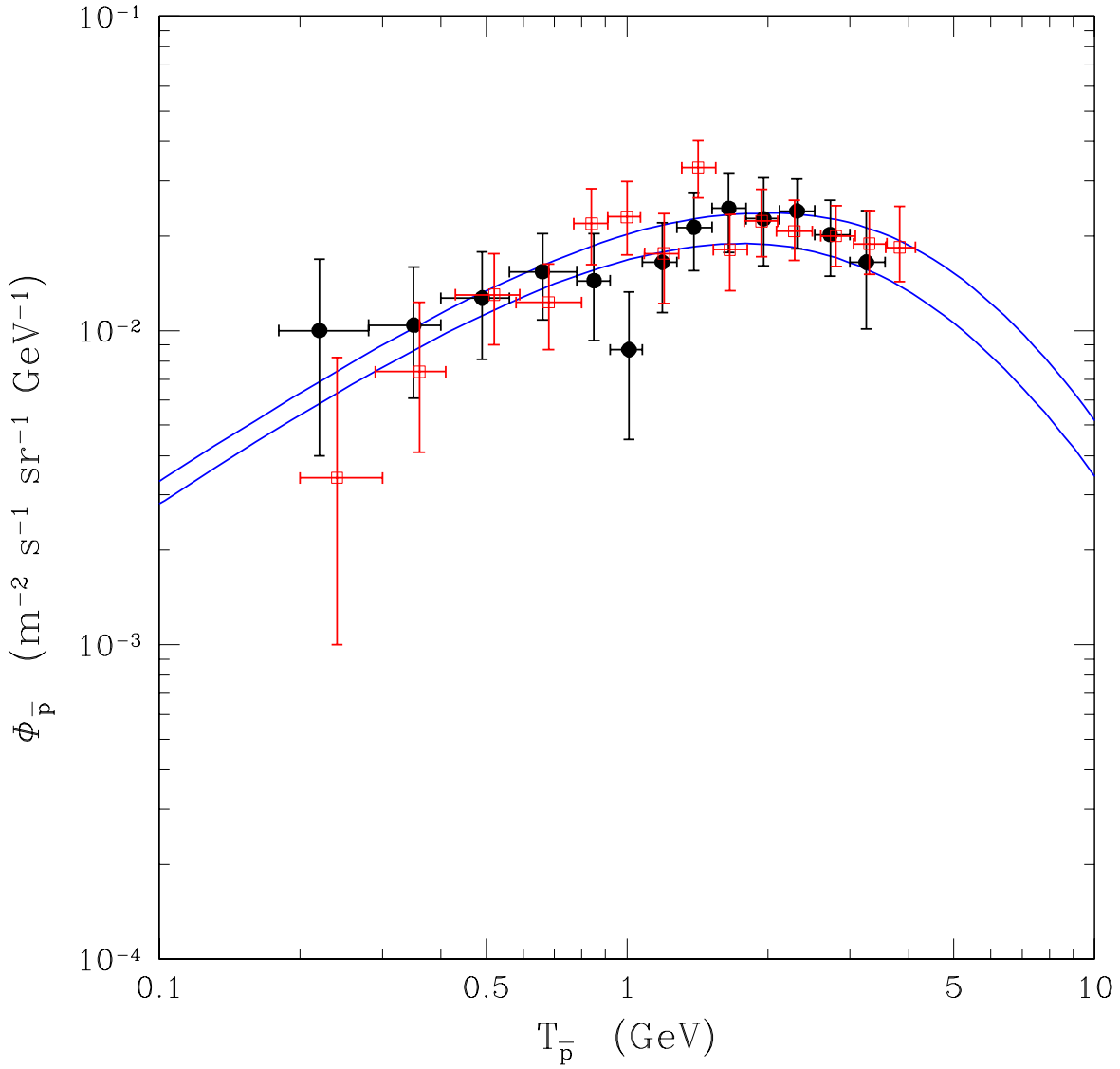

Fig. 7.— Same as previous figure, but where the whole region of parameter space consistent with B/C has been used (Fig. 7 of Paper I). The resulting bounds give an estimation of the uncertainty due to the undeterminacy of the diffusion parameters (data are the same as in Fig. 5).

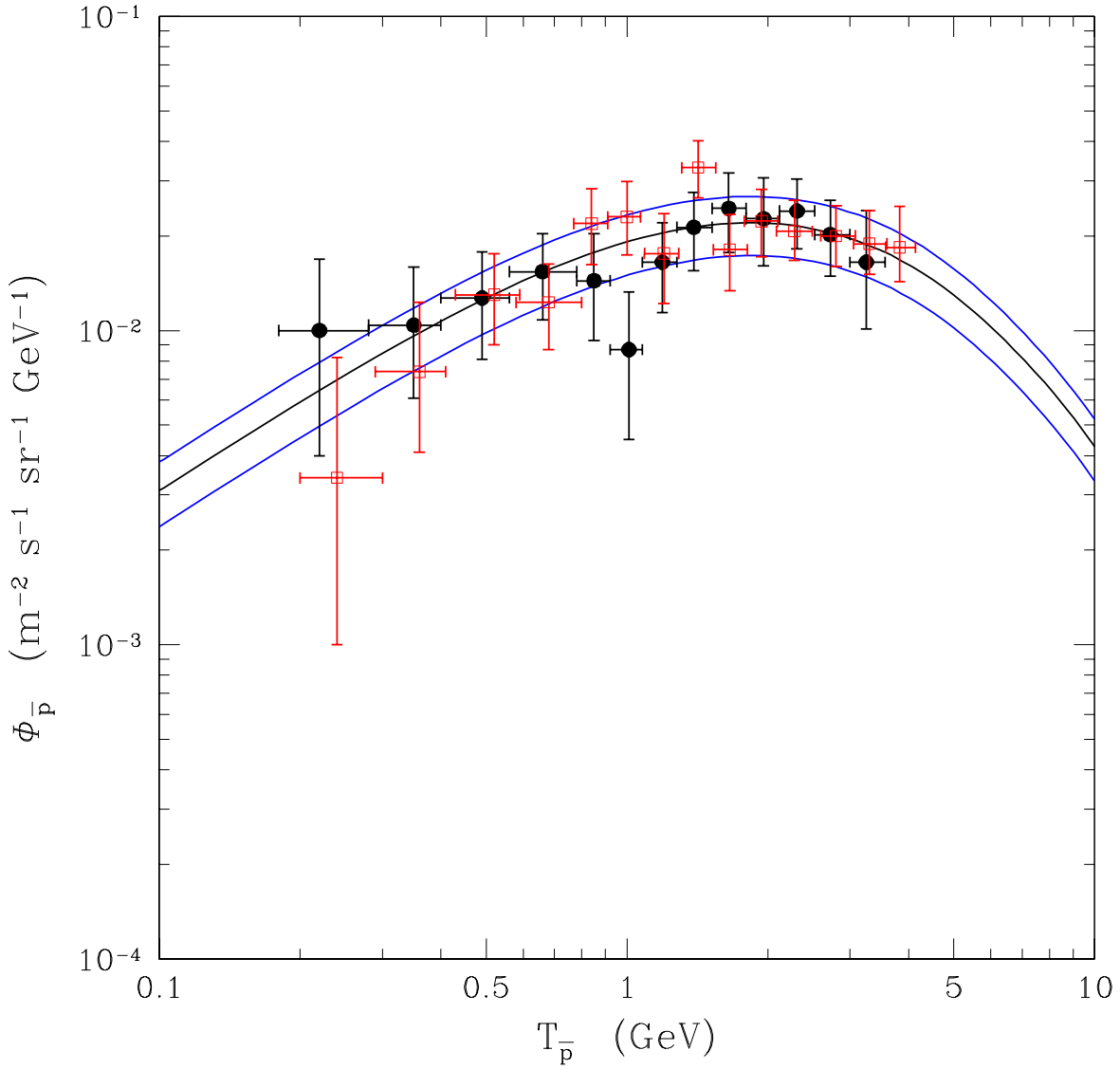

Fig. 8.— In this figure, the TOA antiproton spectrum has been computed with extreme values of DTUNUC nuclear parameters. The central line is the reference curve showed in Fig. 4, while upper and lower curves correspond respectively to the maximum and minimum of the antiproton production rate. These two bounds give an estimation of the uncertainty due to the undeterminacy of the nuclear parameters (data are the same as in Fig. 5).

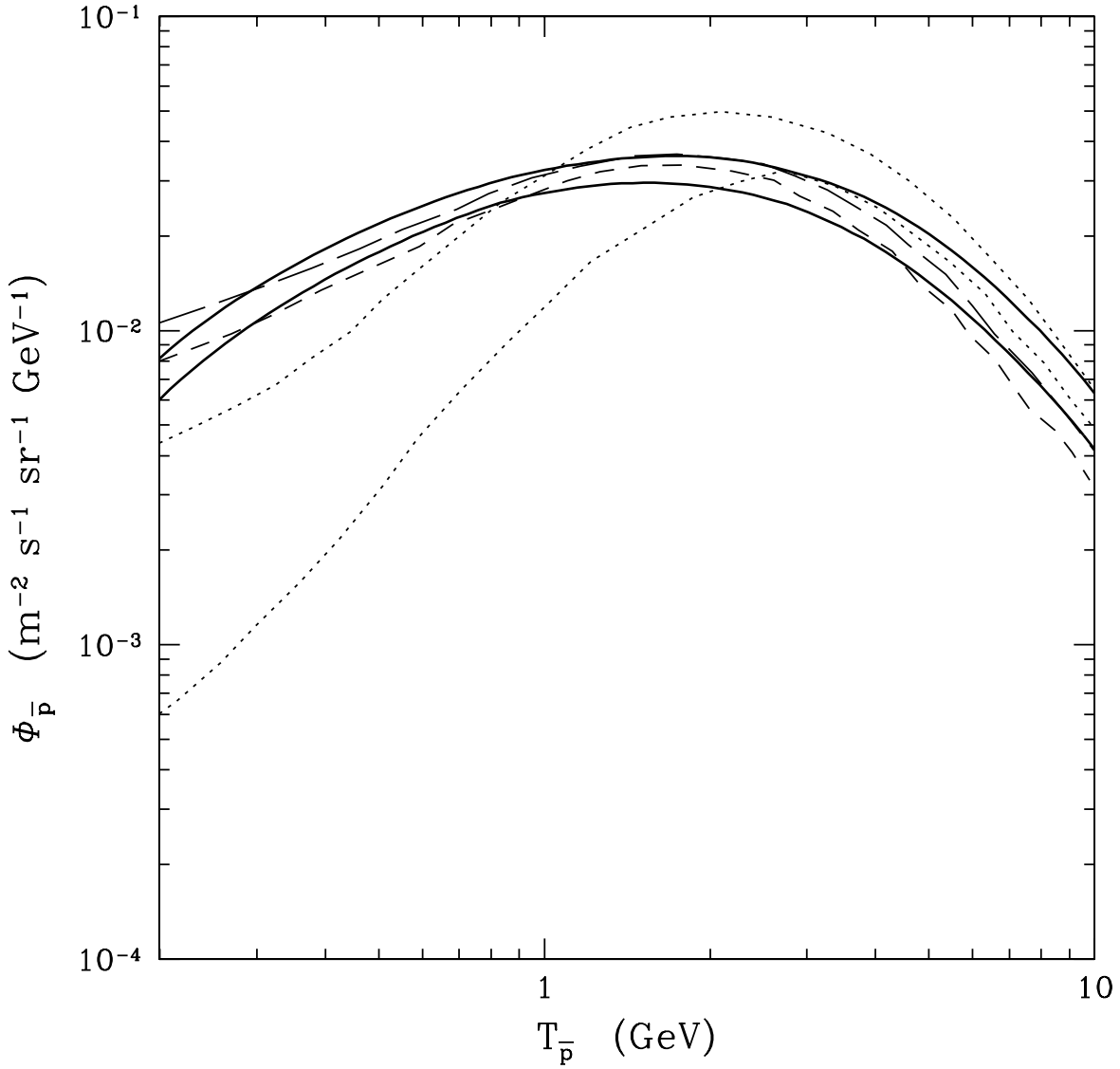

Fig. 9.— Comparison of our interstellar spectra (thick solid lines indicate the lower and upper band due to the uncertainties in the propagation parameters) with other published antiproton spectra. Dotted lines are lower and upper values from Simon et al. (1998), short dashed line is from Bieber et al. (1999) and long dashed line is from Moskalenko et al. (2001).